INTERNATIONAL JOURNAL FOR NUMERICAL METHODS IN FLUIDS
Int. J. Numer. Meth. Fluids 2008; **56**:1625–1651
Published online 7 August 2007 in Wiley InterScience (www.interscience.wiley.com). DOI: 10.1002/fld.1561

Slosh dynamics of inviscid fluids in two-dimensional tanks of various geometry using finite element method

S. Mitra*, †, P. P. Upadhyay and K. P. Sinhamahapatra

Department of Aerospace Engineering, IIT, Kharagpur 721 302, India

SUMMARY

This paper brings into focus some of the interesting effects arising from the motion of the liquid free surface due to sloshing in partially filled containers of several geometrical shapes in two dimensions. The slosh characteristics that include frequencies, free surface profiles and the hydrodynamic pressure over the container walls have been reported in this study. The equations of motion of the fluid, considered inviscid, are expressed in terms of the pressure variable alone. It is assumed that the frequency of the exciting oscillation is not in the immediate neighborhood of the natural slosh frequency, so that the slope of the free surface is small. Simple harmonic oscillation and earthquake excitations are used as the prescribed boundary conditions. A finite difference-based iterative time-stepping technique is employed to advance the solution in the time domain. The paper presents numerical solutions for rectangular, vertically mounted annular cylindrical, trapezoidal and horizontal circular cylindrical containers. Numerical results obtained are compared with the available existing solutions to validate the code developed. The parametric study of the slosh dynamic systems shows the importance of the nature of excitation, fluid height and the geometry of the container. Copyright © 2007 John Wiley & Sons, Ltd.

Received 14 July 2006; Revised 21 May 2007; Accepted 30 May 2007

KEY WORDS: finite element; Galerkin weighted residual method; Newmark's constant-average acceleration method; pressure formulation; earthquake load; sloshing of liquid

INTRODUCTION

Sloshing is a fascinating physical phenomenon characterized by the oscillation of the unrestrained free surface of the liquid in a partially filled container due to external excitation. This phenomenon is of great engineering importance and is associated with several engineering applications, as exemplified by fuel sloshing in liquid propellant launch vehicles, oil oscillation in large storage

*Correspondence to: S. Mitra, Department of Aerospace Engineering, IIT, Kharagpur 721 302, India.
†E-mail: aero_mitra@yahoo.com

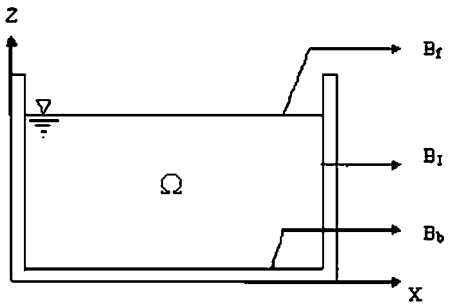

Figure 1. Rectangular tank and its boundaries.

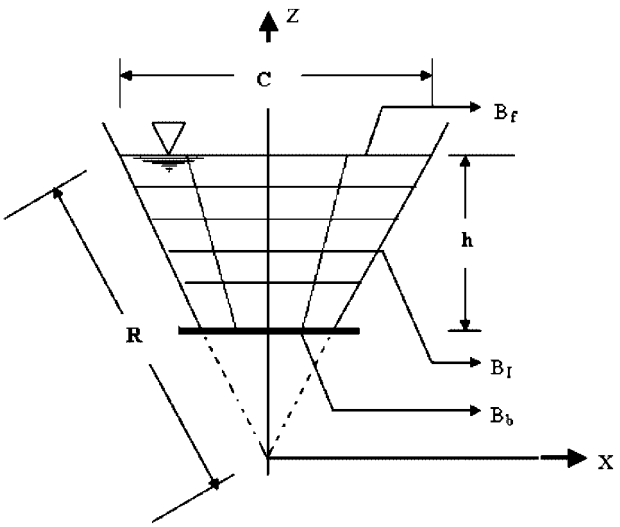

Figure 2. Trapezoidal tank and its boundaries.

tanks, water oscillation in a reservoir and sloshing in the nuclear fuel storage pool due to earthquake and similar other situations. The problem is generally nonlinear, even if the governing equations of the fluid motion is linearized, in the sense that the free surface boundary condition is nonlinear as well as the position of the free surface is not known *a priori*. In spite of that the complete linearization of the system in which the free surface boundary condition is linearized and satisfied on the undisturbed free surface can give satisfactory results in many cases, such as the interaction of small structural motions with acoustic waves in fluids (acoustoelastic fluid–structure interaction model). Although many researchers, References [1–19] amongst others, have accomplished nonlinear simulation successfully, there are numerous successful applications of the linearized theory in the open literature. Exhaustive surveys on both the formulations are included in References [6, 10]. The literature reports a variety of analytical and numerical techniques for formulating linear slosh models for simple rigid and elastic geometries [6, 10, 17, 18, 20–42]. All linear analyses share a common presumption that the disturbance of the free surface is small in magnitude in comparison

DOI: 10.1002/fld

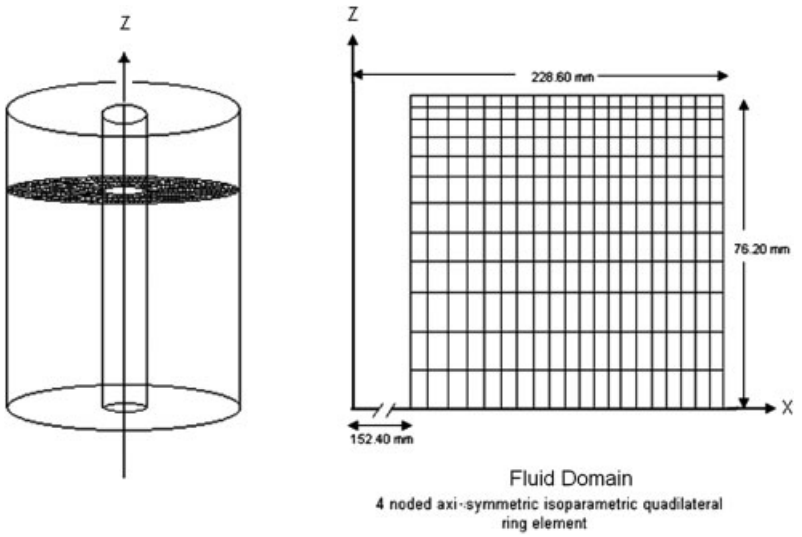

Figure 3. Annular cylindrical configuration with a schematic mesh.

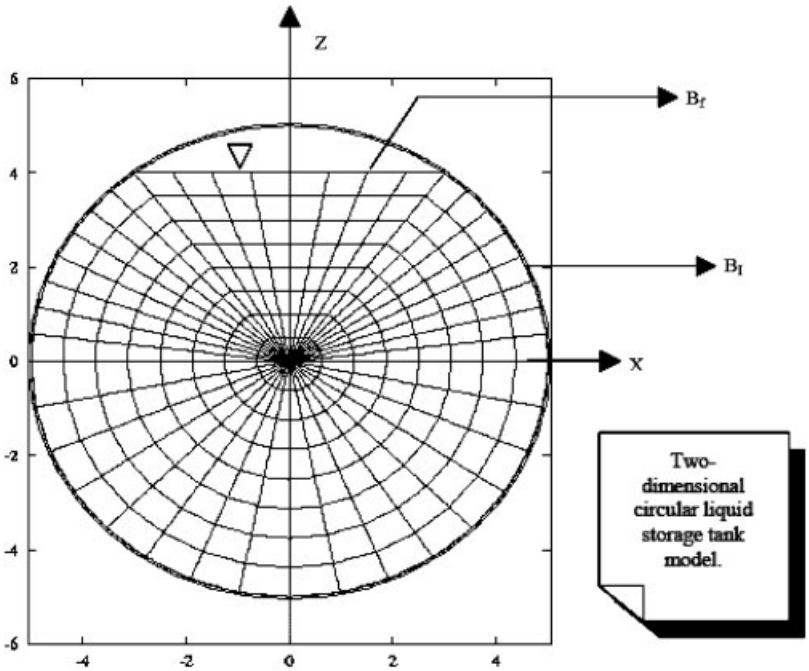

Figure 4. Circular container with fluid boundary definition and schematic mesh.

DOI: 10.1002/fld

Table I. Slosh frequencies (rad/s) in the rectangular container.

Elements per unit length	First mode	Second mode	Third mode
16	5.562	7.921	9.763
25	5.550	7.870	9.725
Stoker [20]	5.541	7.850	9.615

to the liquid depth and the wavelength so that the free surface conditions may be linearized. This has the inherent advantage that the free surface boundary is fixed in time, which simplifies the numerical solution procedure considerably.

Both the linear and nonlinear theories mainly practice two formulations. For liquid sloshing in an elastic container, the structural displacements are almost universal choice as the unknowns for the structure domain. For the fluid, the unknowns are either the displacements, or a force-like quantity, such as the displacement or velocity potential or the pressure. The sloshing response of the fluid–structure system is found to be very sensitive to the characteristics of the ground motion and configuration of the system. Since the earthquakes are unpreventable and unpredictable the only course open to the engineers is to design and built the fluid–structure system so that the loss of property and life can be minimized. For ground excitation dominated by low-frequency contents, the sloshing response increases significantly and the contribution of the higher sloshing modes increases [34, 35]. Since the pioneering works of Dodge *et al.* [1], Miles [21], Bauer [23], Abramson [26] and Housner [27], many research groups have concentrated their investigations on the seismic behaviour of the liquid containers and on the earthquake resistant design to understand the dynamic behaviour of the liquid storage tanks and to provide proper design codes. In spite of the continuous efforts to enhance the performance of liquid containers against seismic loading, many liquid tanks have been severely damaged in major earthquakes all over the world. According to field reports, liquid filled containers are mainly damaged either by excessive axial compression due to overall bending of the containers or by sloshing of the contained liquid with insufficient freeboard between the liquid surface and the tank roof.

While studies on slosh dynamics, both linear and nonlinear, in rectangular and vertically mounted cylindrical tanks are abundant in the open literature, similar studies on trapezoidal and horizontally mounted cylindrical tanks are quite rare. Amongst the few reported studies on trapezoidal and horizontal cylindrical tanks, Bauer [25] and Barnyak [36] have computed sloshing frequencies in a trapezoidal and horizontal cylindrical tanks, respectively. Ortiz and Barhorst [8] have reported a nonlinear boundary element analysis of liquid sloshing in a horizontally mounted circular cylindrical tank. This study presents a numerical method for the analysis of slosh dynamics in rigid storage containers of various geometrical shapes, including trapezoidal and horizontally mounted circular cylindrical tanks in particular, using linearized pressure-based finite element formulation. The characteristics of sloshing behaviour and forced response characteristics have been studied in this paper. In practical applications, one can obtain an approximate solution of the three-dimensional sloshing response from the results of two-dimensional analysis if the third dimension of the cylinder is large. So a two-dimensional analysis will provide an acceptable solution for partially filled long cylinder mounted horizontally.

The fluid domain is discretized using 4-noded quadrilateral elements with pressure as the degree of freedom. However, a layer of triangular elements is employed around the centre of a horizontal

DOI: 10.1002/fld

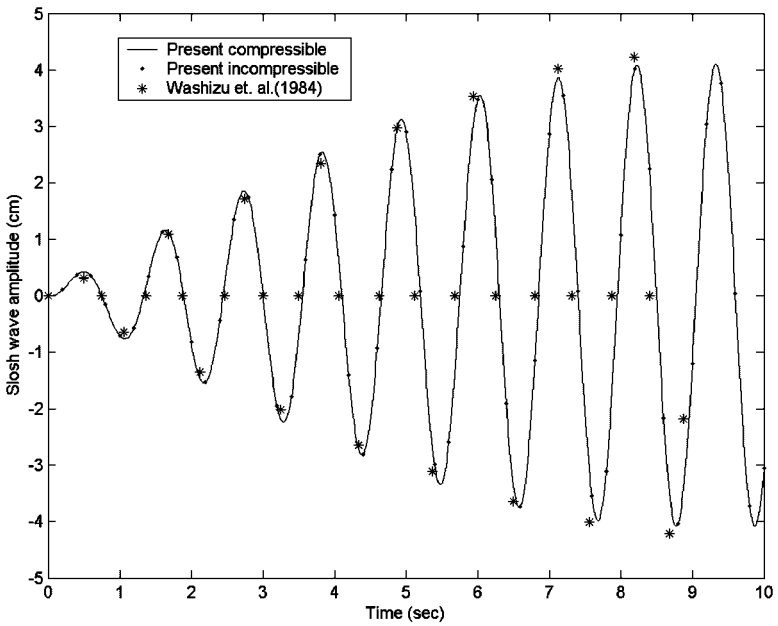

Figure 5. Time histories of the sloshing wave for the rectangular container subject to sinusoidal base excitation.

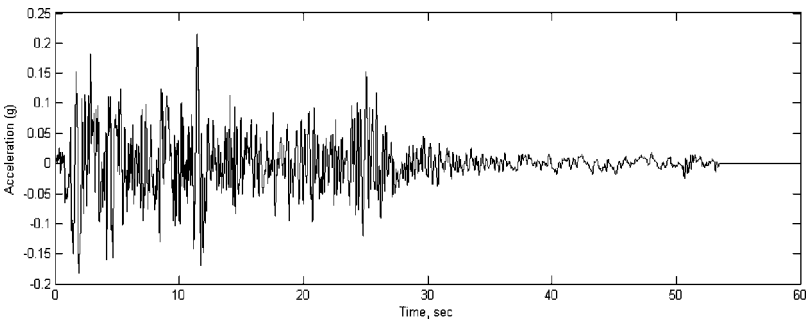

Figure 6. EL Centro earthquake acceleration record (EW component).

circular cylindrical tank. The problem is formulated using the Galerkin principle, which provides the basis for the present spatial discretization. A finite difference-based iterative time-stepping technique is employed to advance the solution in the time domain. Numerical results for the rigid containers are compared with the available existing solutions to assess the accuracy of the developed code. The characteristics of slosh displacement and the hydrodynamic pressure over the container walls for a prescribed earthquake excitation have been reported for containers of various practical geometric shapes.

DOI: 10.1002/fld

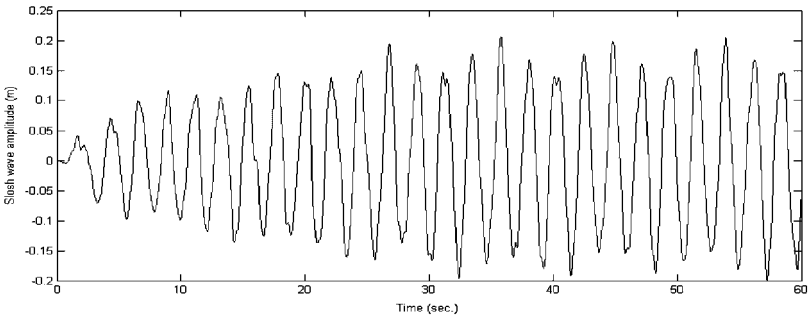

Figure 7. Time histories of the sloshing wave for the rectangular container subject to EW component of EL Centro earthquake.

Table II. Slosh frequencies (Hz) in the annular containers.

	Annular cylindrical Model 1		
Mode	Aslam *et al.* [28]	Pal *et al.* [18]	Present FEM
$M=1$	0.70	0.71	0.74
$M=2$	3.20	3.30	3.24
$M=3$	4.50	4.58	4.56
$M=4$	5.50	5.67	5.58
	Annular cylindrical Model 2		
	Aslam *et al.* [28]	Pal *et al.* [18]	Present FEM
$M=1$	0.90	0.89	0.92
$M=2$	2.30	2.29	2.34
$M=3$	3.20	3.11	3.26
$M=4$	3.90	3.87	3.98

Table III. Peak sloshing displacements (m) in the annular containers.

		Model 1		
Frequency (Hz)	Amplitude of acceleration (g)	Aslam *et al.* [28]	Pal *et al.* [18]	Present FEM
1.20	0.0312	0.004572	0.004688	0.004692
3.70	0.0742	0.006019	0.006179	0.006059
		Model 2		
		Aslam *et al.* [28]	Pal *et al.* [18]	Present FEM
1. 20	0.0312	0.008153	0.007944	0.008263
3.70	0.0742	0.005105	0.005276	0.005150

DOI: 10.1002/fld

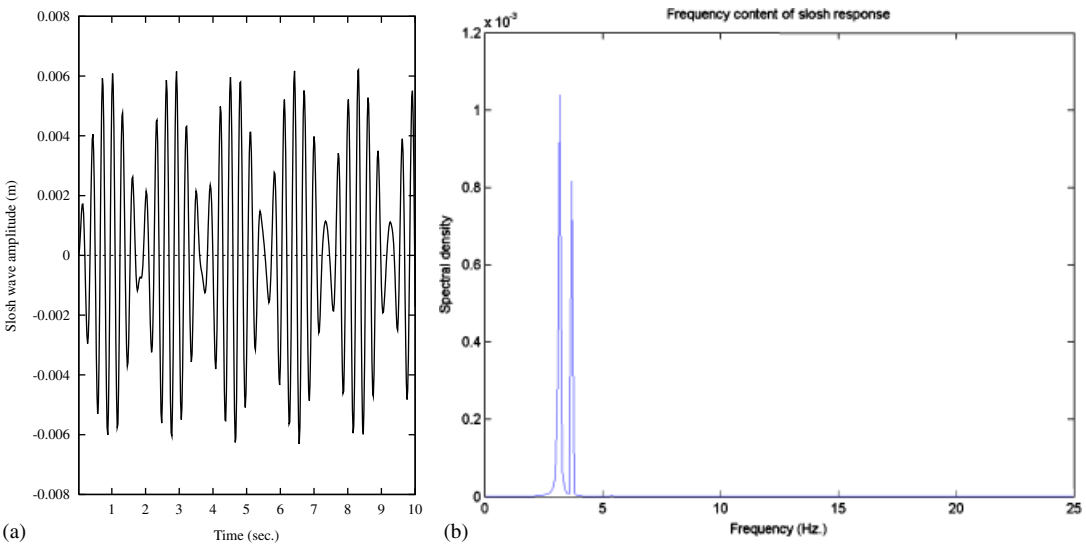

Figure 8. Free surface sloshing response at outer wall of annular cylindrical Model 1 tank under sinusoidal excitation with amplitude $0.0742g$ and frequency 3.7 Hz. (a) Sloshing amplitude variation and (b) spectral analysis of slosh wave amplitude.

GOVERNING EQUATIONS AND FORMULATION

The linearized governing equation for an inviscid, compressible, irrotational flow in terms of excess pressure variable $p(x, z, t)$ is the well-known wave equation, written as

$$\nabla^2 p(x, z, t) = \frac{1}{c^2} \ddot{p}(x, z, t) \quad \text{in } \Omega \tag{1}$$

where Ω is the fluid domain.

The pressure formulation has certain advantages over the displacement or velocity potential-based formulations. Unlike the displacement formulation, the number of unknowns in this formulation is only one per node (pressure), which results in considerable saving of computer storage and time, particularly for large three-dimensional problems. In addition, the pressure field at the structure–fluid interface is directly obtained unlike displacement and potential formulations where the pressure has to be calculated from the velocity or displacements or their potential. This would be particularly advantageous in solving a fluid–structure interaction problem where pressure on the interface needs to be computed at each time step. Besides these major advantages, the compressibility comes in a natural way in a pressure formulation and can be retained without incurring considerable additional efforts and costs. Usually, compressibility proves to be negligible in the general linearized theory of waves on a homogeneous body of liquid. This is also true for all the examples presented in this paper. However, in many practical cases as in the waste storage tanks and spent fuel reprocessing tanks in nuclear facilities, the fluid is inhomogeneous and the density variation is non-uniform but considerable. For the fluid–structure interaction problems, Muller [31] has shown mathematically that eigenvalues of a structure in contact with a compressible fluid are lower than the corresponding eigenvalues if the fluid were incompressible. Muller [31], further,

DOI: 10.1002/fld

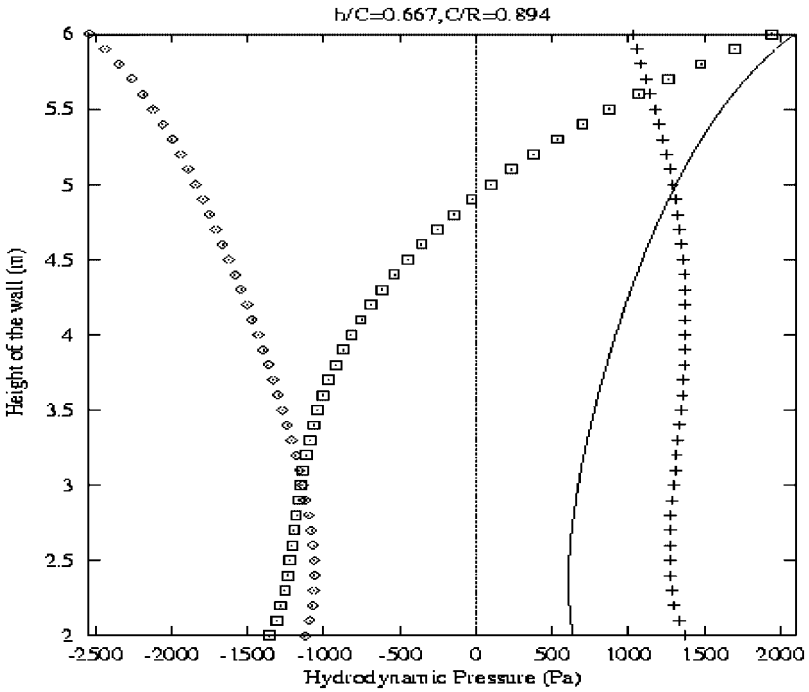

Figure 9. Hydrodynamic pressure variations along a wall of the trapezoidal tank due to a sinusoidal load.

presented a numerical example to show the difference in frequencies considering both air and water as the working fluid. The difference is rather small in the case of water but, perhaps, not negligible.

The fluid boundary, in general, is composed of three types of boundaries. These are solid–liquid interface boundary, free surface boundary, non-reflecting or radiating-type boundary. For liquid sloshing in a container the radiating-type boundary is neglected. Figures 1–4 show different container configurations considered, the relevant boundaries, nomenclatures and definitions. The appropriate boundary conditions for these boundaries are as follows:

1. Solid–liquid interface boundary (B_I): Continuity of normal displacement at the solid–liquid interface leads to the following relation for the linearized problem:

$$\frac{\partial p}{\partial n} = -\rho_f \ddot{u}_n \quad \text{on } B_I \tag{2}$$

2. Free surface boundary (B_f): The linearized wave theory facilitates the satisfaction of the free surface boundary condition on the undisturbed free surface. The free surface boundary conditions are linearized to give

$$p = \rho_f g u_n \tag{3a}$$

$$\Rightarrow \frac{\partial p}{\partial n} = -\frac{\ddot{p}}{g} \quad \text{on } B_f \tag{3b}$$

DOI: 10.1002/fld

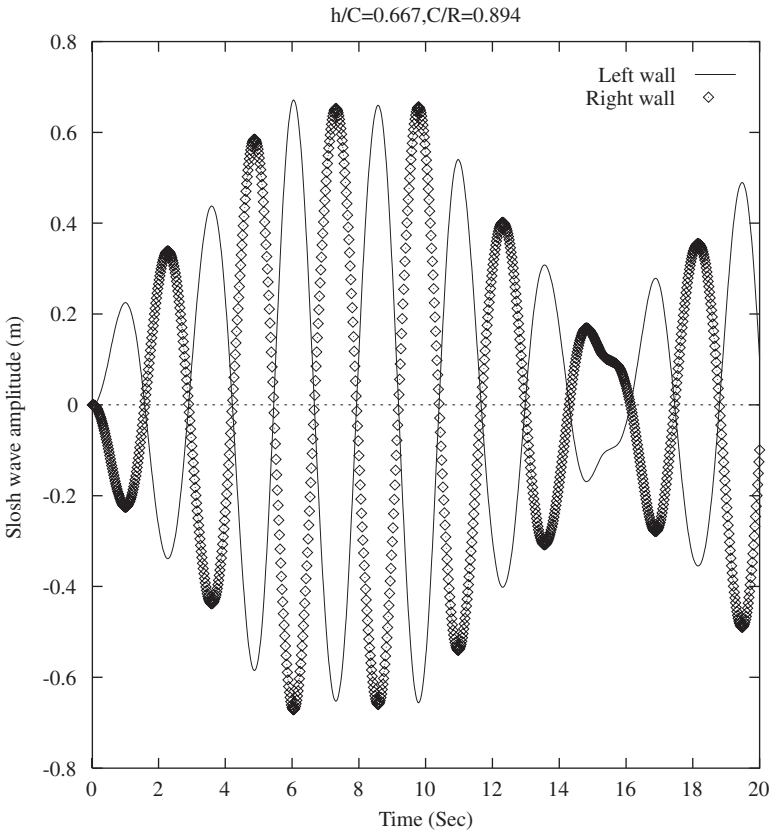

Figure 10. Slosh amplitude at both ends of free surface of the trapezoidal tank due to a sinusoidal load.

3. Bottom boundary (B_b): The bottom boundary is considered to be rigid, so that at the bottom wall of the tank

$$\frac{\partial p}{\partial n} = 0 \quad \text{on } B_b \tag{4}$$

In the above relations ρ_f, $\ddot{u}_n$ and g are the fluid density, normal acceleration of the container wall at the structure–fluid interface and acceleration due to gravity. For a rigid container, the structural acceleration $\ddot{u}_n$ is identical to the prescribed ground acceleration. The parameter c in Equation (1) is the speed of acoustic wave propagation in the fluid. In all the computations reported in this paper c is taken as 1480 m/s, the average speed of sound in water.

Applying the divergence theorem to the residual form of the governing differential equation for the liquid and substituting Equations (2)–(4) we obtain

$$\int_\Omega \overline{N}^T \left[\frac{\partial^2 p}{\partial x^2} + \frac{\partial^2 p}{\partial z^2} - \frac{1}{c^2} \frac{\partial^2 p}{\partial t^2} \right] d\Omega - \int_{B_I} \overline{N}^T \left[\frac{\partial p}{\partial n} + \rho_f \ddot{u}_n \right] d\Gamma - \int_{B_f} \overline{N}^T \left[\frac{\partial p}{\partial n} + \frac{\ddot{p}}{g} \right] d\Gamma = 0 \tag{5}$$

DOI: 10.1002/fld

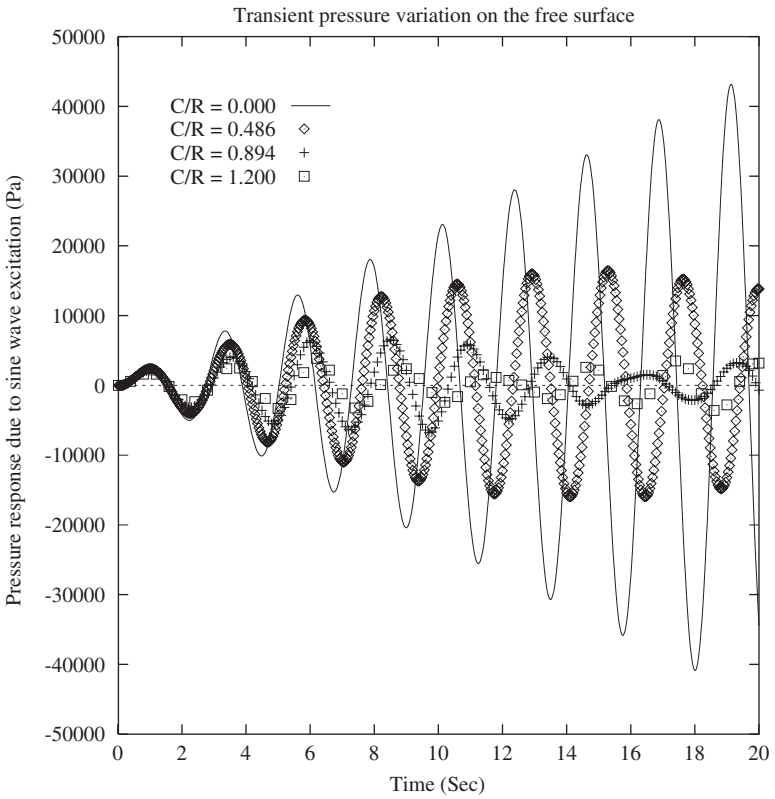

Figure 11. Pressure responses of trapezoidal tank of various C/R ratios due to sinusoidal load.

in which $B = B_{\mathrm{I}} + B_{\mathrm{f}} + B_{\mathrm{b}}$ is as defined in Figures 1–4. As there is no bottom boundary in the case of circular domain (Figure 4) the total boundary consists of interface and free surface boundaries only. The use of Green–Gauss theorem and Galerkin finite element approximation reduces the above equation to the following form:

$$M_{\mathrm{f}}\ddot{\overline{p}} + K_{\mathrm{f}}\overline{p} = F \tag{6}$$

The parameter M_{f} in Equation (6) is the mass matrix for a fluid element and is given by

$$(M_{\mathrm{f}})_{ij} = \frac{1}{c^2}\int_{\Omega} N_{\mathrm{f}_i}^{\mathrm{T}} N_{\mathrm{f}_j}\,\mathrm{d}\Omega + \frac{1}{g}\int_{B_{\mathrm{f}}} N_{\mathrm{f}_i}^{\mathrm{T}} N_{\mathrm{f}_j}\,\mathrm{d}\Gamma \tag{7}$$

Similarly, K_{f}, the stiffness matrix for a fluid element, is given by

$$(K_{\mathrm{f}})_{ij} = \int_{\Omega}\left(\frac{\partial N_{\mathrm{f}_i}}{\partial x}\frac{\partial N_{\mathrm{f}_j}}{\partial x} + \frac{\partial N_{\mathrm{f}_i}}{\partial z}\frac{\partial N_{\mathrm{f}_j}}{\partial z}\right)\mathrm{d}\Omega \tag{8}$$

DOI: 10.1002/fld

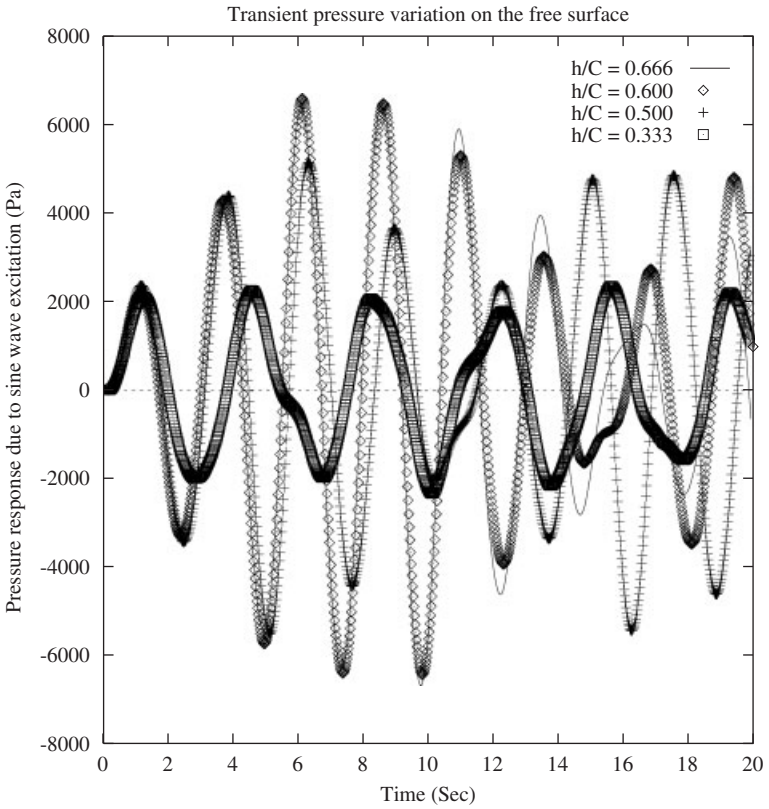

Figure 12. Pressure responses for different h/C ratios.

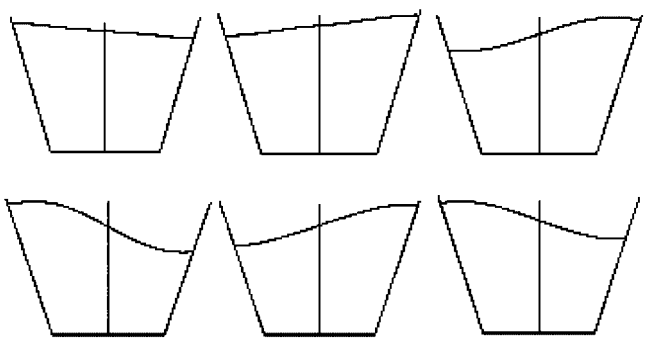

Figure 13. Free surface profiles at 1, 2, 5, 6, 9 and 11 s due to the sinusoidal load.

The load vector, F, is given by

$$F_i = \int_{B_\mathrm{I}} N_{\mathrm{f}_i}^{\mathrm{T}} \rho_\mathrm{f} \ddot{u}_\mathrm{n} \, \mathrm{d}\Gamma \tag{9}$$

DOI: 10.1002/fld

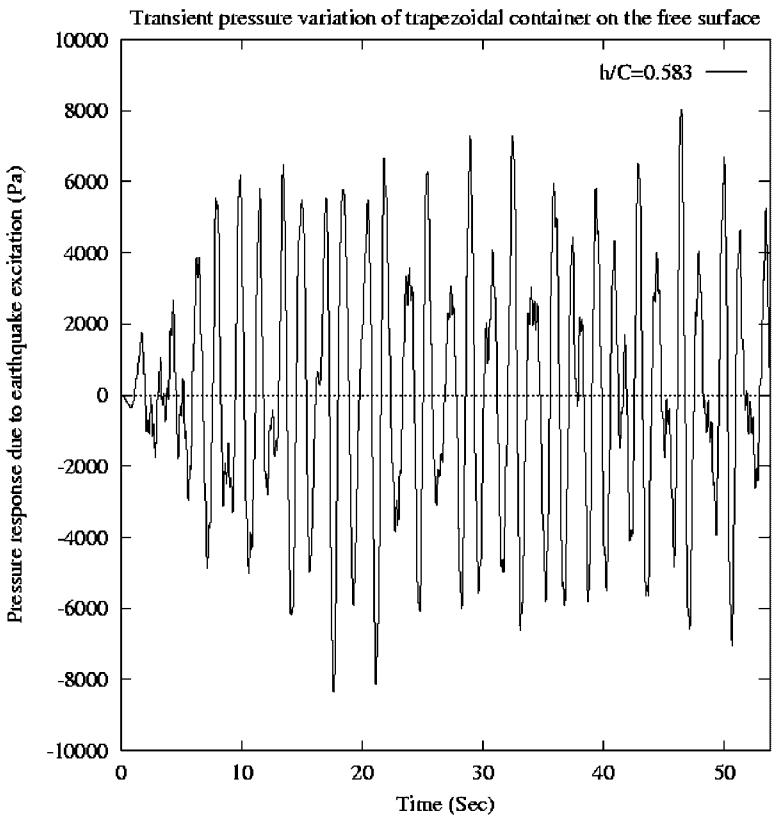

Figure 14. Transient pressure variation due to El Centro earthquake.

For an incompressible formulation the first term on the right-hand side in Equation (7) vanishes. The discretized governing equation (6) is solved using a finite difference-based time-stepping technique, namely, Newmark's constant-average acceleration method [37]. The solution is advanced assuming an initial undisturbed condition (zero excess pressure). At each time step the set of algebraic equations are solved using a skyline LDL^T solver.

FLUID IN AXISYMMETRIC CONTAINERS

The horizontal ground motion will excite only the antisymmetric modes of sloshing in an axisymmetric tank if linearized free surface condition is used. The pressure in this case may be expressed in the form of a Fourier cosine series. The fluid element is essentially a ring element and the element stiffness matrix may be expressed as

$$(K_m)_{ij} = \int_0^{2\pi} \cos^2 \theta R(\xi)(K_f)_{ij}\, d\theta \tag{10}$$

DOI: 10.1002/fld

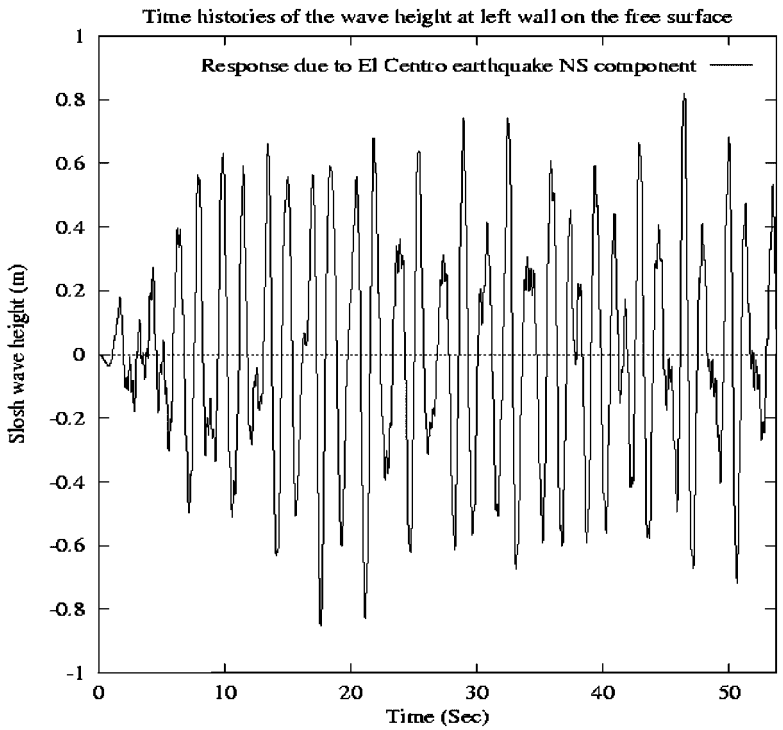

Figure 15. Transient slosh wave height.

where R is the radius vector of the element under consideration and $(K_f)_{ij}$ is the stiffness matrix of the non-axisymmetric fluid element as obtained earlier. Similarly, the mass matrix and the load vector for an axisymmetric element may be obtained from their non-axisymmetric counterpart.

FREE SURFACE POSITION

In the linearized analysis the free surface boundary conditions are satisfied on the initial undisturbed position. Hence, it is not essential to update the free surface and computational mesh at each time step. However, it is necessary to compute the displacements of the surface nodes to plot the free surface position. In the present analysis, Equation (3a) is used directly to deduce the free surface displacement for all vertical walled containers. When the container walls are not vertical, as in the cases of trapezoidal and horizontal cylindrical containers, the free surface nodal displacements are computed from the velocity components of the nodal fluid particles. The components of the acceleration of the fluid particles are obtained from the following inviscid flow equations:

$$\rho_f \dot{v}_i + p_{,i} = 0, \quad i = x, z \tag{11}$$

where $\dot{v}_i$ is the acceleration of the fluid particle. The velocity components of the fluid particles are evaluated from the known values of acceleration at any instant of time using simple time

DOI: 10.1002/fld

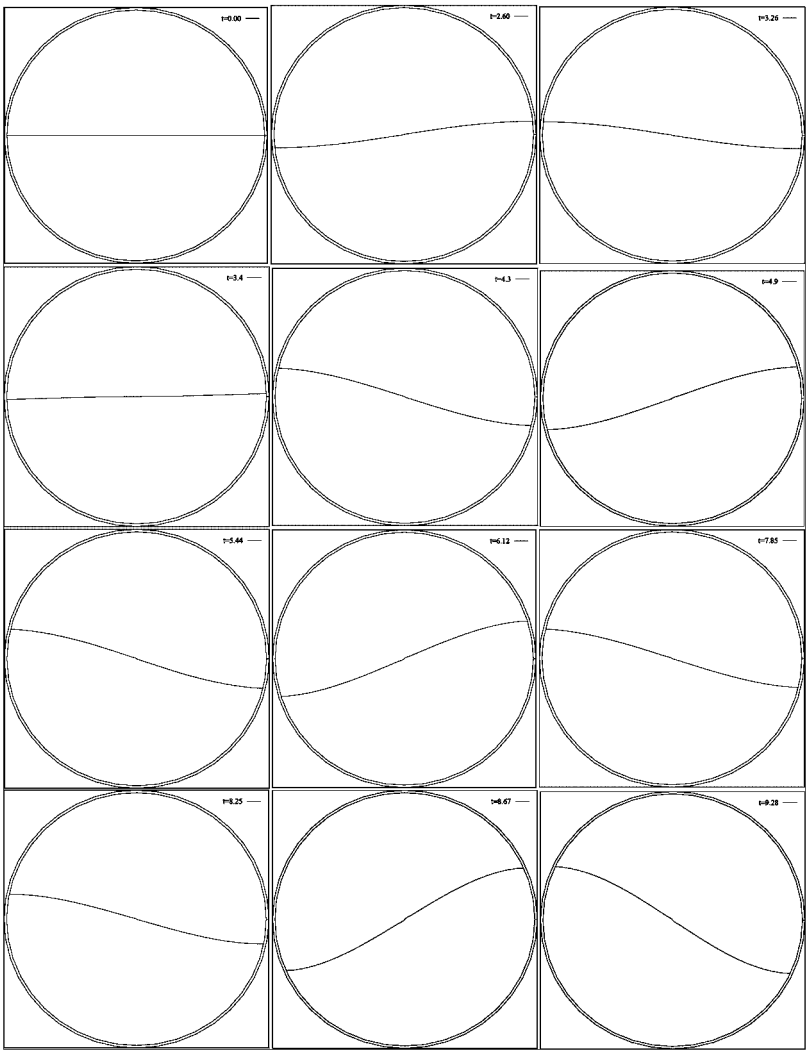

Figure 16. Motion with zero damping (displacement amplitude $A = -0.01$ m, $\omega = 5$ rad/s).

integration scheme given by

$$v_t = v_{t-\Delta t} + \dot{v}_t \Delta t \tag{12}$$

The nodal displacements are computed from the velocities in a similar manner. Finally, if the end nodes are found to be off the walls, they are moved along the normal to put them on the walls.

DOI: 10.1002/fld

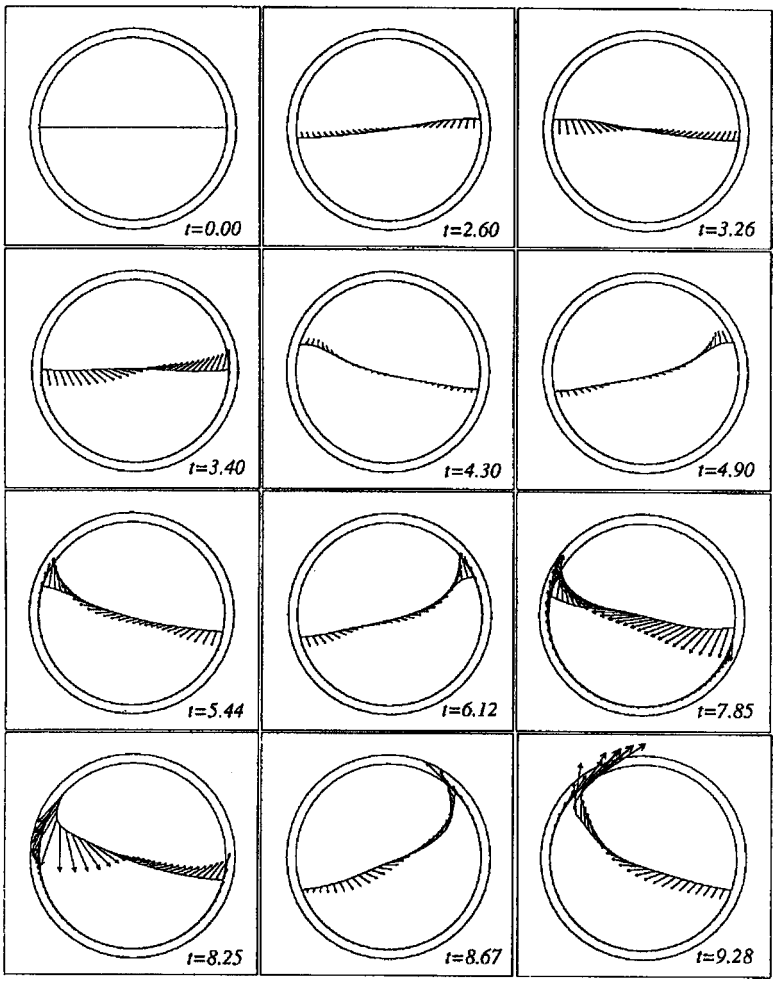

Figure 17. Motion with zero damping ($A = -0.01\,\text{m}, \omega = 5\,\text{rad/s}$) (Courtesy of Ortiz and Barhorst [8]).

Table IV. Sloshing frequencies (Hz) of a 50% filled horizontal cylindrical tank of radius 0.5 m.

First mode (f_1)	Second mode (f_2)	Third mode (f_3)	Fourth mode (f_4)	Fifth mode (f_5)
0.8205	1.2274	1.5198	1.7605	1.9712

NUMERICAL EXAMPLES AND DISCUSSION

Rectangular containers

The benchmark problem of liquid sloshing inside a 1.0 m wide rectangular rigid container with liquid domain size of 1.0 m × 1.0 m is attempted to validate the developed code and to assess the

DOI: 10.1002/fld

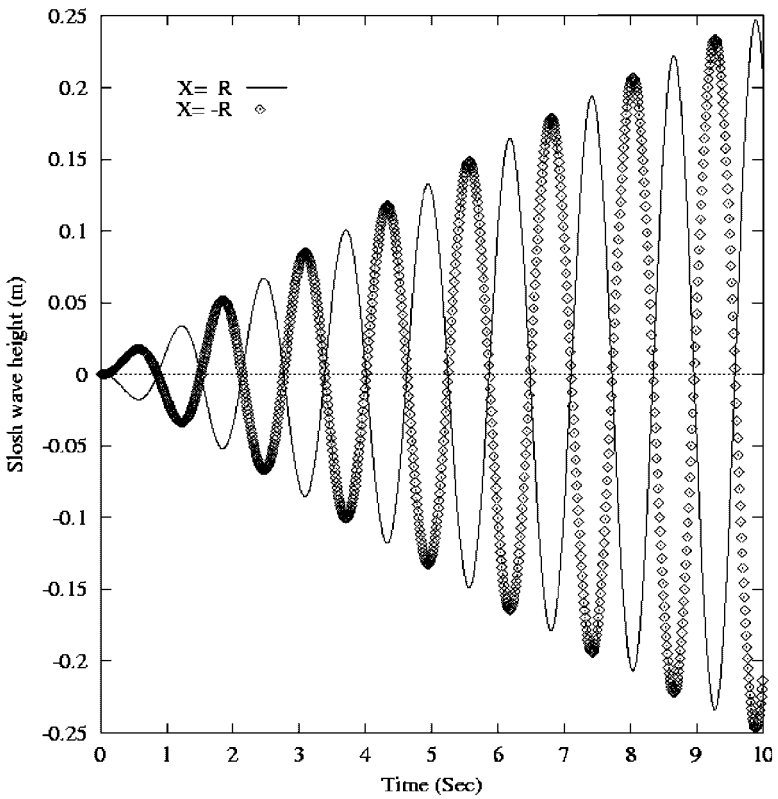

Figure 18. Time histories of the wave height at both the walls.

accuracy of the numerical method adopted. The computed results presented in Table I for the first three sloshing frequencies of the liquid (water) inside the rectangular container are found to match closely with the solution due to Stoker [20].

Typical time response of the free surface wave height for the same rectangular container at the left wall is shown in Figure 5 for the situation when the amplitude and frequency of the applied harmonic (sine) base acceleration are $0.02\,\mathrm{m/s^2}$ and $5.5\,\mathrm{rad/s}$, respectively, i.e. $\ddot{u}_n = 0.02 \sin 5.5t$. The response shown in the figure appears to match closely with that due to Washizu *et al.* [4]. Both incompressible and compressible solutions are presented in the figure and the figure shows, as expected, that the two solutions are practically identical for this case. The effect of close proximity between the fundamental sloshing frequency and the excitation frequency is noticeable in the increase in amplitude of the sloshing waves.

The rectangular configuration (container width 1.0 m with liquid depth of 1.0 m) studied for the validation purpose has been further investigated for the slosh dynamics due to an earthquake load, namely the EW component of the EL Centro earthquake (Figure 6). Figure 7 represents the surface wave amplitude at the right wall of the container. It is clearly observed from the response to a strong earthquake motion, like the EL Centro earthquake, that the maximum hydrodynamic pressure and the slosh wave amplitude are amplified markedly compared with the response to the

DOI: 10.1002/fld

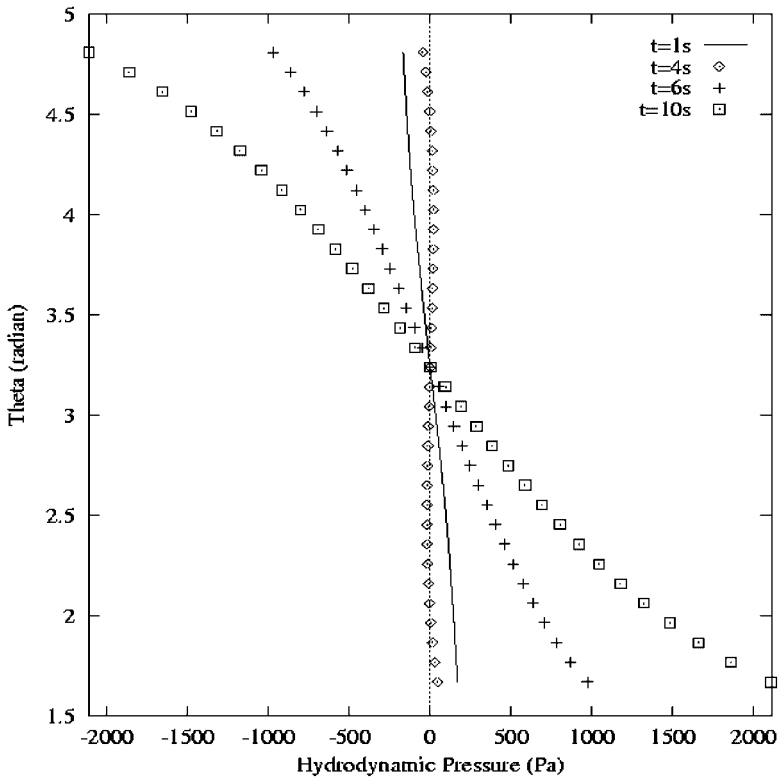

Figure 19. Hydrodynamic pressure distribution at different instants ($R = 0.5$ m, half fill).

sinusoidal excitation given earlier. However, considering the fact that the peak ground acceleration for this earthquake is nearly 100 times, the rise in hydrodynamic pressure is rather small since the excitation and sloshing frequencies are quite apart in this case.

Upright annular cylindrical containers

The liquid sloshing inside a vertically mounted annular cylindrical container is also considered to validate the code. Two containers have been used in the present study. These are designated as Model 1 having outer radius 0.2286 m, inner radius 0.1524 m, depth of liquid 0.0762 m and Model 2 having outer radius 0.2286 m, inner radius 0.0762 m and depth of liquid 0.0762 m. The numerical results presented in Table II for the first four sloshing frequencies are found to match closely with the velocity potential-based finite element method (FEM) solution due to Pal *et al.* [18] and the experimental results due to Aslam *et al.* [28]. In Table III the computed values of the maximum slosh displacement at the free surface for two different harmonic sinusoidal excitations are presented. The computed slosh displacements are found to match quite satisfactorily with other solutions for both the excitations. The slosh wave height variation with time at the outer wall of the tank (Model 1) subjected to a harmonic excitation of amplitude $0.0742g$ and frequency of 3.7 Hz ($\ddot{u}_n = 0.0742g \sin 23.2478t$) is shown in Figure 8, which clearly reveals a time interference of two waves having small difference in their frequencies. An FFT spectrum analysis shows that

DOI: 10.1002/fld

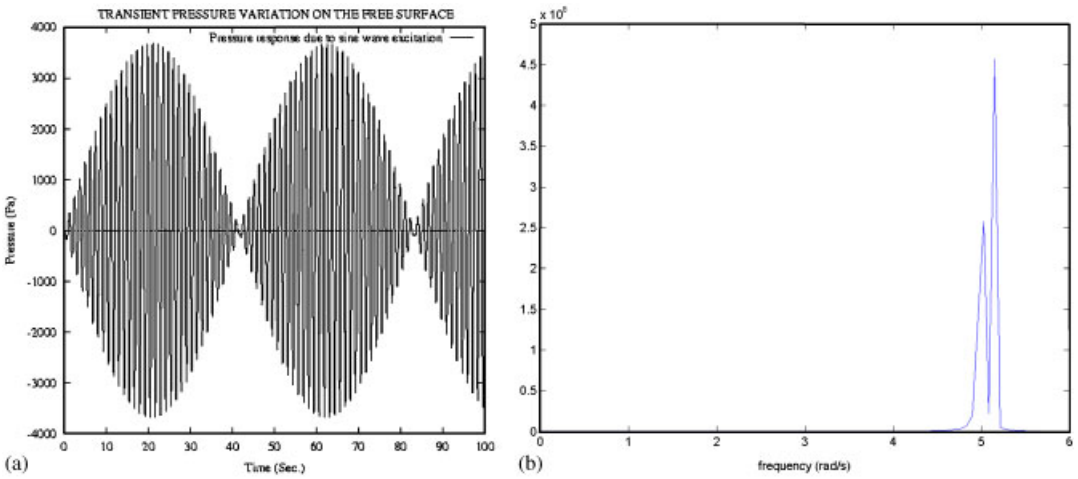

Figure 20. (a) Pressure response on the free surface of circular container due to sinusoidal load and (b) spectrum analysis of the free surface pressure response.

the frequencies contributing to the beating behaviour are 3.7 Hz (excitation frequency) and 3.2 Hz (second mode natural frequency) and both of them have almost equal contribution.

Trapezoidal containers

Some studies have also been carried out for trapezoidal containers with varying C/R and h/C ratios (Figure 2) due to sinusoidal and earthquake excitations. Figure 9 presents the hydrodynamic pressure distribution along the wall of a trapezoidal tank with C/R ratio of 0.894 at various instants due to the sinusoidal load of amplitude $1.0\,\mathrm{m/s^2}$ and frequency of 0.4424 Hz. The depth of liquid in the tank is taken to be 4.0 m with $h/C = 0.667$. The fundamental sloshing frequency for this configuration is computed to be 2.39 rad/s. As mentioned above, the harmonic excitation is taken as $\ddot{u}_n = 1.0 \sin 2.78t$. The slosh response in the form of slosh wave height variation with time at the left and right intersection points between the container walls and the free surface is shown in Figure 10. It is observed that for the container with $C/R = 0.894$, $h/C = 0.667$ and $h = 4.0$ m, the peak slosh wave amplitude increases during the first 10 s and then decreases for the next 5 s and then continues to increase again till the computation is terminated at 20 s from the start. Figure 11 presents the transient pressure variation at the left wall intersection of a number of trapezoidal containers subjected to the same harmonic excitation, namely $\ddot{u}_n = 1.0 \sin 2.78t$. In each of these cases, the depth of liquid is fixed at 4.0 m and C and R are changed in such a way that the liquid volume too remains unchanged. It is evident from Figure 11 that the hydrodynamic pressure and, hence, the slosh height decreases markedly as the ratio C/R increases. The large difference with the rectangular container ($C/R = 0$) is worth mentioning. This significant reduction in the slosh amplitude and pressure can be attributed to the fact that only a component of the load is responsible for the sloshing in a trapezoidal container. Figure 12 shows the pressure variation at the left extreme of the free surface for varying liquid depths in a fixed container. Liquid depths of 1.0, 2.0, 3.0 and 4.0 m so that the h/C ratios are 0.333, 0.5, 0.6 and 0.666, respectively, are considered for this study. The effect of liquid depth on the sloshing response is found to be quite

DOI: 10.1002/fld

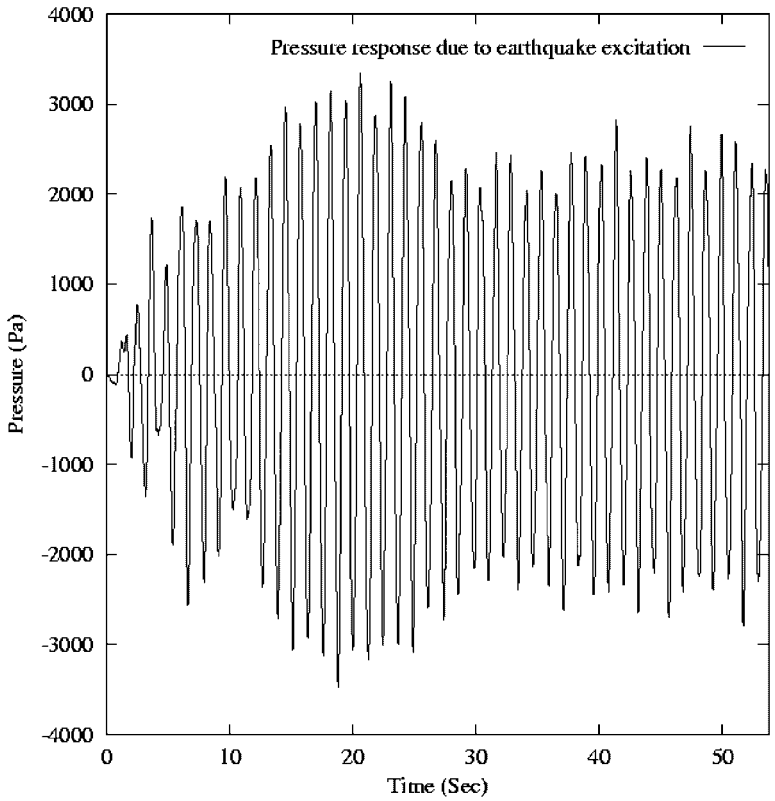

Figure 21. Pressure response on the free surface at the right wall due to NS component of El Centro earthquake load.

complex. The phenomenon of interference in time is noticeable for all the cases except the lowest depth. The difference in the interfering frequencies appears to be decreasing with increasing h and h/C. For the lowest depth case, the difference seems to be so large that the interference is practically absent. This case also shows distinctly larger period of oscillation. The free surface profiles of the container with $C/R = 0.486$ and $h = 4.0\,\text{m}$ at different time instants are shown in Figure 13.

The effect of earthquake excitation on the sloshing amplitude and the hydrodynamic pressure in a trapezoidal container is studied with a prescribed ground motion corresponding to the NS component of the El Centro earthquake. The tank configuration considered in this case is characterized by $C/R = 1.2$, $h/C = 0.583$ and the liquid depth $h = 3.5\,\text{m}$. Figures 14 and 15 show the transient pressure variation and the surface wave amplitudes, respectively. The relatively higher values of the peak hydrodynamic pressure and sloshing amplitude are expected since the excitation contains considerably larger peaks. However, the maximum free surface displacement is within 20% of the undisturbed liquid depth and the linearized theory would be quite acceptable.

DOI: 10.1002/fld

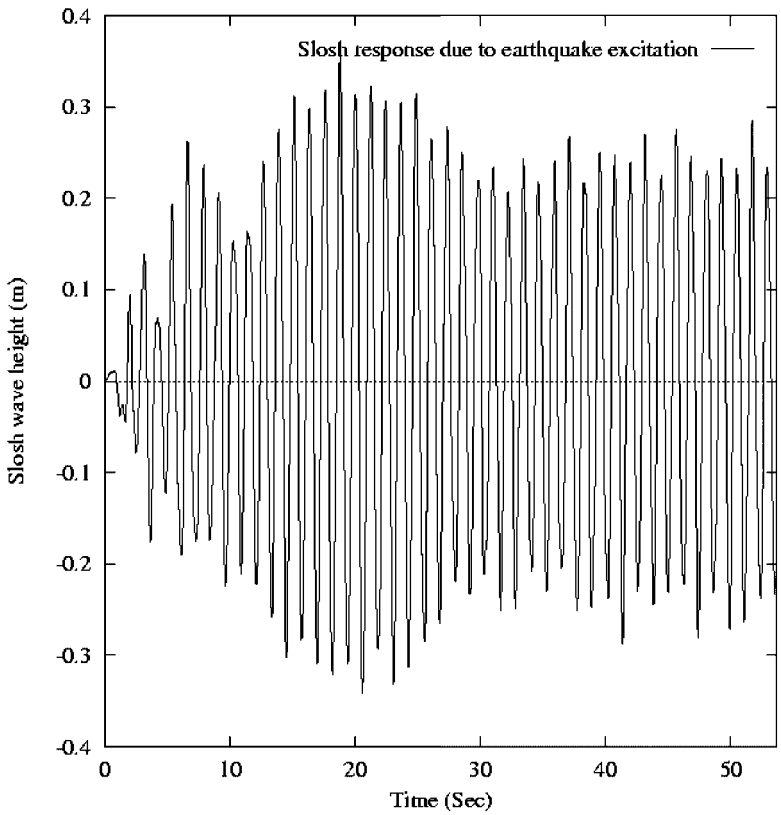

Figure 22. Wave height at the left wall on the free surface due to NS component of El Centro earthquake load.

Circular containers (*horizontal cylindrical containers*)

The present numerical solution for a half-filled horizontal cylindrical tank of radius 0.5 m subjected to a sinusoidal excitation $u_n = A \sin(\omega t)$ with displacement amplitude $A = -0.01$ m and frequency $\omega = 5$ rad/s is compared with the nonlinear velocity potential-based boundary element solution due to Ortiz and Barhorst [8]. The time step in the present computation is taken as 0.01 s for advancing the solution. The fluid domain is discretized using 3965 four-noded quadrilateral elements and 72 triangular elements around the centre. Figure 16 shows plots of the free surface position for the half-filled container at different instants for the prescribed excitation. The corresponding solution due to Ortiz and Barhorst [8] is reproduced from Reference [8] in Figure 17. The results are found to be in excellent agreement up to 8.0 s from the start of the motion. Beyond this time, some discrepancies in the free surface position are observed. These discrepancies may be attributed to the limitations of the present linear formulation. Ortiz and Barhorst [8] predicted unstable response of the system beyond 9.85 s but the present technique is found to be capable of capturing the slosh response beyond that time. Although the FEMs are usually more robust than the boundary element method employed by Ortiz and Barhorst [8], the nonlinearity may have significant effect

DOI: 10.1002/fld

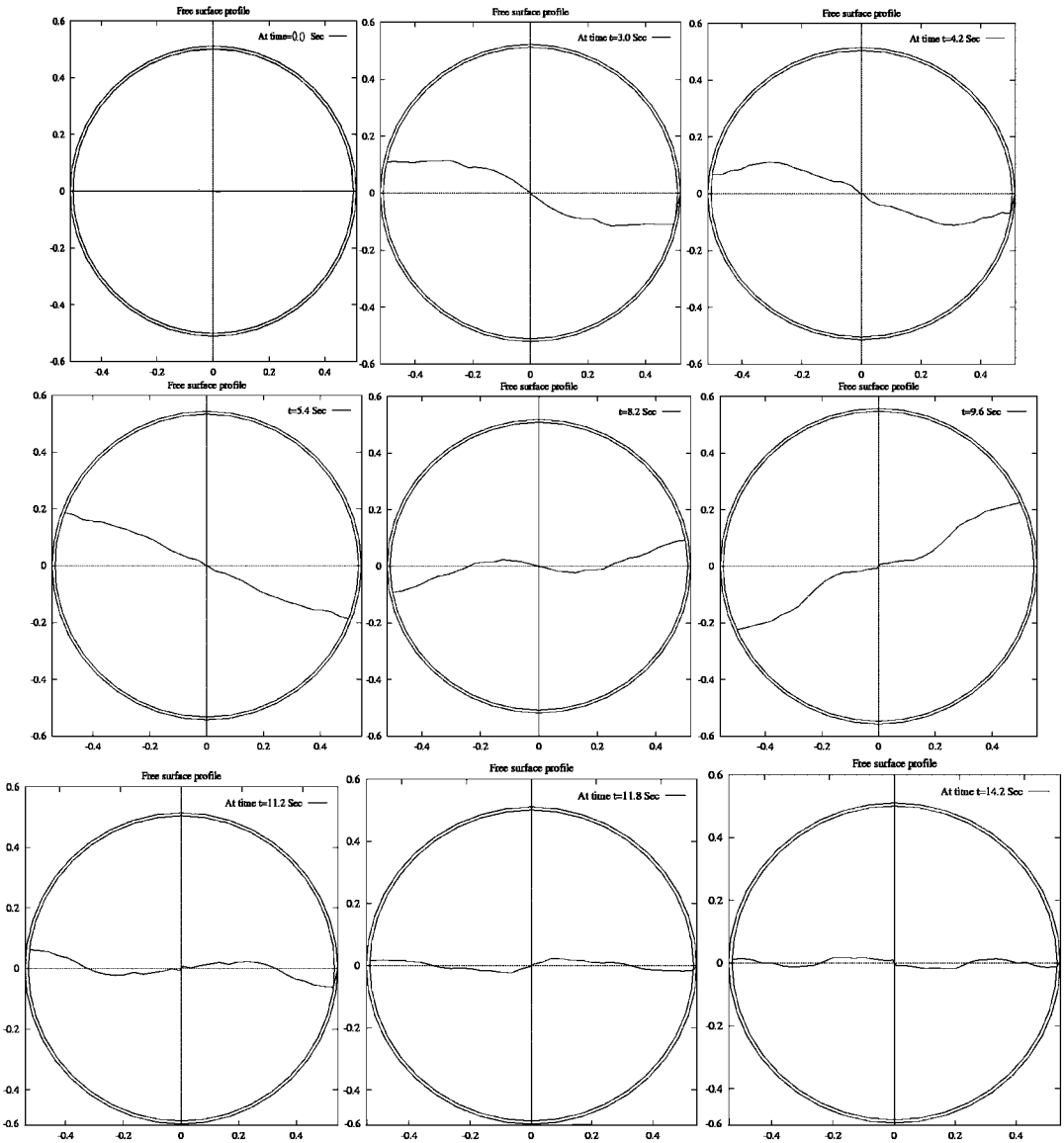

Figure 23. Motion due to NS component of El Centro earthquake at 0, 3, 4.2, 5.4, 8.2, 9.6, 11.2, 11.8 and 14.2 s.

as the displacements tend to be quite large during this period. As evident from the system natural frequencies presented in Table IV, the fundamental sloshing frequency in this case is very close to the exciting frequency and, consequently, the sloshing amplitudes are expected to be large enough. In spite of that, the predictions seem to be quite close to the nonlinear solution up to 8.0 s.

DOI: 10.1002/fld

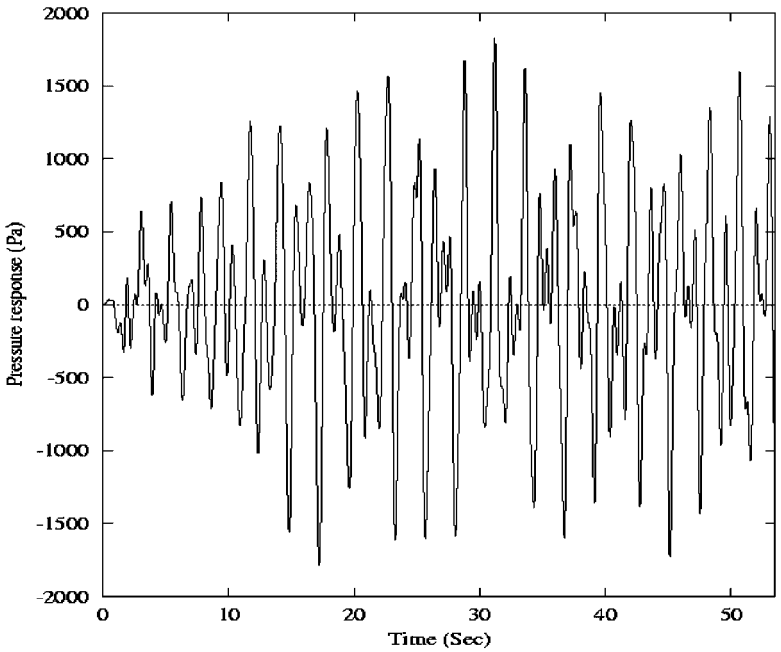

Figure 24. Pressure history of the 75% filled container due to the NS component of El Centro earthquake.

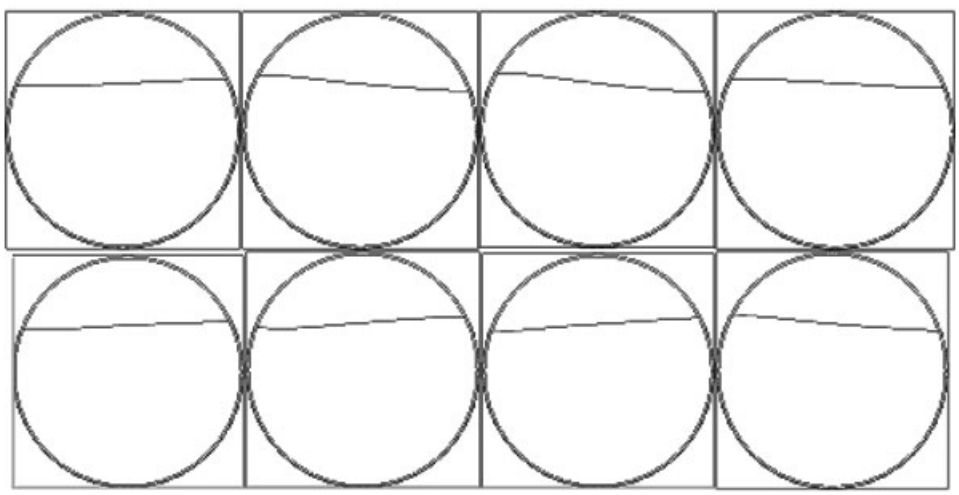

Figure 25. Free surface profiles at 1, 3, 4, 8, 10, 12, 16 and 18 s due to sinusoidal load (75% fill).

Transient slosh wave height variation on the free surface position at both the walls of a half-filled horizontal circular cylindrical tank of radius 0.5 m is plotted in Figure 18. The excitation considered in this case is given as $u_n = A\sin(\omega t)$ with $A = -0.01$ m and $\omega = 5.0$ rad/s. The corresponding

DOI: 10.1002/fld

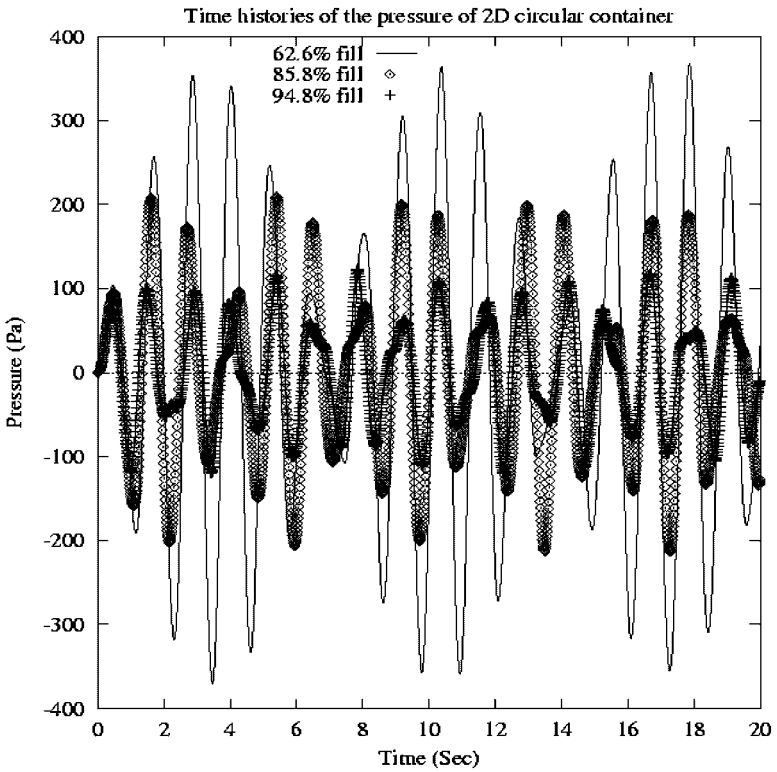

Figure 26. Transient pressure variation for varying liquid volumes.

hydrodynamic pressure distributions on the wall at different instants are shown in Figure 19. The angle θ is measured from the Z-axis (Figure 4) in clockwise direction for every node on the wall. The free surface pressure variation at the left intersection, which is similar to the slosh height variation there, is shown in Figure 20(a) for the first 100 s. The characteristic beating behaviour in response over a large time is due to the contributing frequencies of 5.0 rad/s (exciting frequency) and 5.2 rad/s (natural sloshing frequency). The respective contributions of the two frequencies are shown in the spectrum analysis in Figure 20(b). As mentioned earlier (Table IV), the fundamental sloshing frequency in this case is quite close to the excitation frequency and the slosh wave amplitudes and the hydrodynamic pressure values are quite large. Therefore, this example serves as a critical test case for the code. It is found from the figure, which clearly shows an interference, that the peak pressure and wave amplitude rise during the first 20 s to considerably large values and the free surface displacement to the undisturbed liquid depth ratio is more than 0.5 during 10–20 s.

Subsequently, the slosh dynamic response of the above tank system to the NS component of the El Centro earthquake has been taken up for further investigations. The time variations of the pressure and the slosh wave height on the free surface are presented in the Figures 21 and 22. The hydrodynamic pressure in the figure (Figure 21) is taken at the intersection between the right wall and the free surface while the slosh height (Figure 22) is taken at the intersection point between

DOI: 10.1002/fld

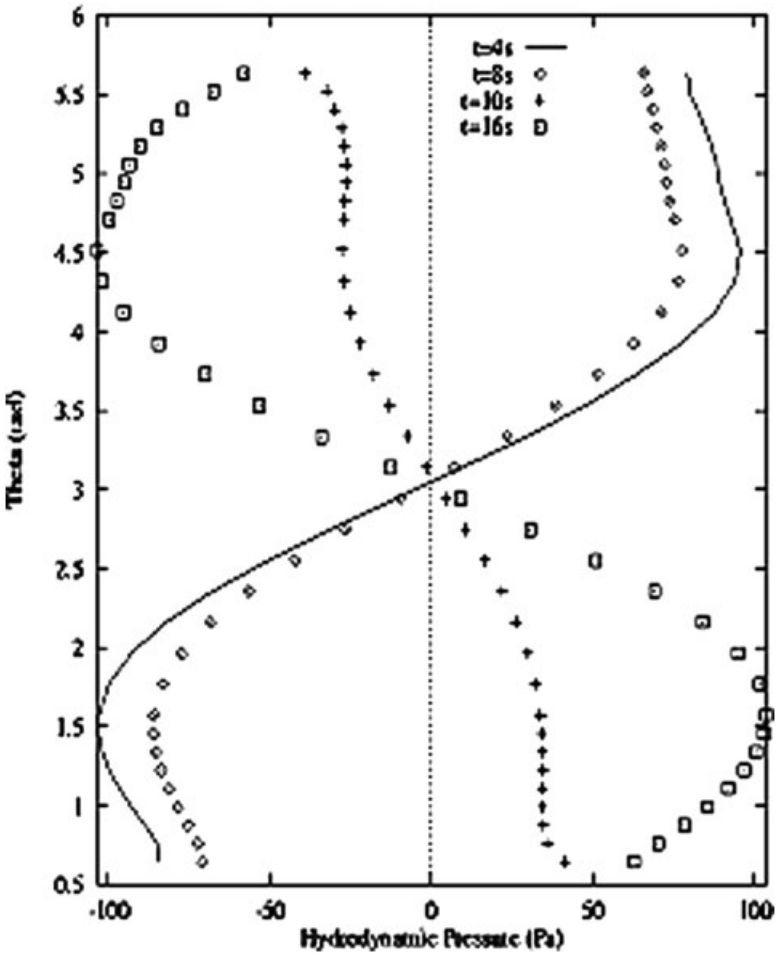

Figure 27. Hydrodynamic pressure distribution.

the left wall and the free surface. It is understood from the figures that the maximum pressure and slosh height occur between 19 and 20 s. The peak pressure in this case is somewhat smaller than that of the sinusoidal excitation considered above. This difference may be attributed to the difference in the excitation frequencies. The free surface profiles at a number of instances are presented in Figure 23. Transient pressure variation on the free surface of the 75% filled circular container of radius 0.5 m subjected to the NS component of the El Centro earthquake is presented in Figure 24. The figure clearly indicates a marked reduction in the peak hydrodynamic pressure and, consequently, in the sloshing amplitude.

Figure 25 depicts the free surface profiles at different instants for the circular container when it is 75% filled due to the sinusoidal excitation used for the half-filled case. It is found that the maximum free surface displacement is appreciably lower than that of the half-filled container. Figure 26 presents a comparison of free surface pressure variation in 62.6, 85.8 and 94.8% filled

DOI: 10.1002/fld

circular tanks due to the same sinusoidal excitation. With the increase in the liquid depth or volume in the container, noticeable reduction in the free surface pressure is observed. This is, probably, due to the increased sloshing frequency of the system and consequent difference with the excitation frequency. As an example, the fundamental sloshing frequency of the 75% filled container is found to be 1.044 Hz compared with 0.8205 Hz of the half-filled container and is far removed from the excitation frequency of 0.7958 Hz. Figure 27 presents the hydrodynamic pressure variations along the wall at 4, 8, 10 and 16 s for the 94.8% filled container. The angle θ is measured from the Z-axis (Figure 4) in clockwise direction for every node on the wall.

CONCLUSION

A pressure-based Galerkin finite element code that can handle liquid sloshing analysis for a free lateral vibration of ground-supported containers of various practical shapes has been developed. The slosh dynamics in long horizontal circular cylindrical and trapezoidal containers, which are relatively scarce in the open literature, is given special attention in this study. The analysis is restricted to linear problems in the sense that only small amplitude waves have been assumed. The method has been applied to a number of problems and some typical results are presented that assess the accuracy and applicability of the method.

Trapezoidal containers have an advantage of reducing slosh when compared with the rectangular containers. With an increase in the inclination of the slant walls with respect to the vertical, the slosh wave amplitude and pressure reduce markedly for a fixed liquid height and volume. For more than 50% filled horizontal circular cylindrical containers, it is observed, the slosh response decreases considerably with an increase in the liquid height.

The developed computer code is useful in predicting the sloshing displacement and the pressure developed in a liquid filled container due to sloshing. The predictions of the free surface displacement and the hydrodynamic pressure on the wall due to sloshing are effective in deciding the level of liquid in tanks, fixing the level of an outlet pipe in a boiler suppression pool and in overall design of the liquid filled containers.

REFERENCES

1. Dodge FT, Kana DD, Abramson HN. Liquid surface oscillations in longitudinally excited rigid cylindrical containers. *AIAA Journal* 1965; **3**(4):685–695.
2. Dodge FT, Garza LR. Simulated low gravity sloshing in spherical, ellipsoidal and cylindrical tanks. *Journal of Spacecraft and Rockets* 1970; **7**(1):204–206.
3. Miles JW. Wave motion in a viscous fluid of variable depth: moving contact line. *Journal of Fluid Mechanics* 1991; **223**:47–55.
4. Washizu K, Nakayama T, Ikegewa M, Yoshikazu T, Adachi T. Some finite element techniques for the analysis of nonlinear sloshing problems. In *Finite Elements in Fluids*, Gallaghar RH, Oden JT, Zenkiewicz OC, Kawai T, Kawahara M (eds), vol. 5. Wiley, 1984; 357–376.
5. Dodge FT, Abramson HN. Liquid propellant dynamics in the SATURN/APOLLO vehicles—a look back. *AIAA Paper 2000-1676*, 2000.
6. Morand HJP, Ohayon R. *Fluid–Structure Interaction*: *Applied Numerical Methods*. Wiley: New York, 1995.
7. Chen W, Haroun MA, Liu F. Large amplitude liquid sloshing in seismically excited tanks. *Earthquake Engineering and Structural Dynamics* 1996; **25**:653–669.
8. Ortiz JL, Barhorst AA. Large-displacement non-linear sloshing in 2D circular rigid containers—prescribed motion of the container. *International Journal for Numerical Methods in Engineering* 1998; **41**:195–210.

DOI: 10.1002/fld

9. Ibrahim RA, Pilipchuk VN, Ikeda T. Recent advances in liquid sloshing dynamics. *Applied Mechanics Reviews* (ASME) 2001; **54**(2):133–199.
10. Ibrahim RA. *Liquid Sloshing Dynamics*: *Theory and Applications*. Cambridge University Press: Cambridge, MA, 2005.
11. Faltinsen OM, Timokha AN. Asymptotic modal approximation of nonlinear resonant sloshing in a rectangular tank with small fluid depth. *Journal of Fluid Mechanics* 2002; **470**:319–357.
12. Turnbull MS, Borthwick AGL, Eatock Taylor R. Numerical wave tank based on a σ-transformed finite element inviscid flow solver. *International Journal for Numerical Methods in Fluids* 2003; **42**:641–663.
13. Frandsen JB. Sloshing motion in excited tanks. *Journal of Computational Physics* 2004; **196**(1):53–87.
14. Cariou A, Casella G. Liquid sloshing in ship tanks: a comparative study of numerical simulation. *Marine Structures* 1999; **12**:183–189.
15. Celebi MS, Akyuldiz H. Nonlinear modeling of liquid sloshing in moving rectangular tank. *Ocean Engineering* 2002; **29**:1527–1553.
16. Wu GX, Ma QA, Eatock Taylor R. Numerical simulation of sloshing waves in a 3D tank based on a finite element method. *Applied Ocean Research* 1998; **20**:337–355.
17. Abramson HN. Dynamics of contained liquids: a personal odyssey. *Applied Mechanics Reviews* 2003; **56**(Part I):R1–R7.
18. Pal NC, Bhattacharya SK, Sinha PK. Nonlinear coupled slosh dynamics of liquid filled laminated composite containers: a two-dimensional approach. *Journal of Sound and Vibration* 2003; **261**:729–749.
19. La Rocca M, Sciortino G, Adduce C, Boniforti MA. Experimental and theoretical investigation on the sloshing of a two-liquid system with free surface. *Physics of Fluids* 2005; **17**:062101.
20. Stoker J. *Water Waves*. Interscience: New York, 1957.
21. Miles JW. On the sloshing of liquid in a flexible tank. *Journal of Applied Mechanics* 1958; **25**(2):277–283.
22. Isaacson M, Ryu, Chung-Son. Earthquake-induced sloshing in vertical container of arbitrary section. *Journal of Engineering Mechanics* (ASCE) 1998; **124**(2):158–166.
23. Bauer HF. Theory of fluid oscillations in a circular cylindrical ring tank partially filled with liquid. *NASA-TN-D-557*, 1960.
24. Bauer HF, Eidel W. Frictionless liquid sloshing in circular cylindrical container configurations. *Aerospace Science and Technology* 1999; **3**:301–311.
25. Bauer HF. Oscillations of non-viscous liquid in various container geometries. *Forschungbericht LRT-WE-9-FB-1*, 1999.
26. Abramson HN. Dynamic behaviour of liquid in moving containers. *Applied Mechanics Reviews* (ASME) 1963; **16**(7):501–506.
27. Housner GW. The dynamic behavior of water tanks. *Bulletin of the Seismological Society of America* 1963; **53**(2):381–387.
28. Aslam M, Godden WG, Scalise DT. Earthquake sloshing in annular and cylindrical tanks. *Journal of Engineering Mechanics* (ASCE) 1979; **EM3**:371–389.
29. Zienkiewicz OC, Bettes P. Fluid–structure dynamic interaction and wave forces—an introduction to numerical treatment. *International Journal for Numerical Methods in Engineering* 1978; **13**:1–16.
30. Olson LG, Bathe KJ. A study of displacement-based fluid finite elements for calculating frequencies of fluid and fluid–structure systems. *Nuclear Engineering and Design* 1983; **76**:137–151.
31. Muller WC. Simplified analysis of linear fluid–structure interaction. *International Journal for Numerical Methods in Engineering* 1981; **17**:113–121.
32. Haroun MA. Earthquake response of deformable liquid storage tanks. *Journal of Applied Mechanics* (ASME) 1981; **48**(2):411–418.
33. Kim JK, Koh HM, Kwahk IJ. Dynamic response of rectangular flexible fluid containers. *Journal of Engineering Mechanics* 1996; **122**(9):807–817.
34. Choun YS, Yun CB. Sloshing characteristics in rectangular tanks with a submerged block. *Computers and Structures* 1996; **61**(3):401–413.
35. Choun YS, Yun CB. Sloshing analysis of rectangular tanks with a submerged structure by using small-amplitude water wave theory. *Earthquake Engineering and Structural Dynamics* 1999; **28**:763–783.
36. Barnyak OM. Normal oscillations of viscous liquid partially filling a circular horizontal channel. *International Applied Mechanics* 1997; **33**(4):335–343.
37. Klaus-Jurgen Bathe. *Finite Element Procedures*. Prentice-Hall: Englewood Cliffs, NJ, 1996.
38. Cho JR, Song JM, Lee JK. Finite element techniques for the free-vibration and seismic analysis of liquid-storage tanks. *Finite Elements in Analysis and Design* 2001; **37**:467–483.

DOI: 10.1002/fld

39. Cho JR, Song JM. Assessment of classical numerical models for the separate fluid–structure modal analysis. *Journal of Sound and Vibration* 2001; **239**(5):995–1012.
40. Maity D, Bhattacharyya SK. A parametric study on fluid–structure interaction problems. *Journal of Sound and Vibration* 2003; **263**:917–935.
41. Chen JZ, Kianoush MR. Seismic response of concrete rectangular tanks for liquid containing structures. *Canadian Journal of Civil Engineering* 2005; **32**:739–752.
42. Kianoush MR, Mirzabozorg H, Ghaemian M. Dynamic analysis of rectangular liquid containers in three-dimensional space. *Canadian Journal of Civil Engineering* 2006; **33**:501–507.

DOI: 10.1002/fld